Defects in Vestibular Sensory Epithelia and Innervation in Mice with Loss of *Chd7* Function: Implications for Human CHARGE Syndrome

MEREDITH E. ADAMS,[1] ELIZABETH A. HURD,[2] LISA A. BEYER,[1] DONALD L. SWIDERSKI,[1] YEHOASH RAPHAEL,[1] AND DONNA M. MARTIN[2,3]*
[1]Department of Otolaryngology, The University of Michigan, Ann Arbor, Michigan, 48109
[2]Department of Human Genetics, The University of Michigan, Ann Arbor, Michigan, 48109
[3]Department of Pediatrics, The University of Michigan, Ann Arbor, Michigan, 48109

ABSTRACT

CHD7 is a chromodomain gene mutated in CHARGE syndrome, a multiple anomaly condition characterized by ocular coloboma, heart defects, atresia of the choanae, retarded growth and development, genital hypoplasia, and ear defects including deafness and semicircular canal dysgenesis. Mice with heterozygous *Chd7* deficiency have circling behavior and semicircular canal defects and are an excellent animal model for exploring the pathogenesis of CHARGE features. Inner ear vestibular defects have been characterized in heterozygous *Chd7*-deficient embryos and early postnatal mice, but it is not known whether vestibular defects persist throughout adulthood in *Chd7*-deficient mice or whether the vestibular sensory epithelia and their associated innervation and function are intact. Here we describe a detailed analysis of inner ear vestibular structures in mature mice that are heterozygous for a *Chd7*-deficient, gene-trapped allele ($Chd7^{Gt/+}$). $Chd7^{Gt/+}$ mice display variable asymmetric lateral and posterior semicircular canal malformations, as well as defects in vestibular sensory epithelial innervation despite the presence of intact hair cells in the target organs. These observations have important functional implications for understanding the clinical manifestations of *CHD7* mutations in humans and for designing therapies to treat inner ear vestibular dysfunction. J. Comp. Neurol. 504:519–532, 2007.

Indexing terms: mouse mutant; inner ear; innervation; sensory epithelia

CHD7, a recently identified chromodomain gene, is mutated in human CHARGE syndrome, a multiple congenital anomaly condition characterized by ocular coloboma, heart defects, atresia of the choanae, retarded growth and development, genital hypoplasia, and ear abnormalities including deafness and vestibular dysfunction, and brainstem/cranial nerve dysfunction (Lin et al., 1990; Byerly and Pauli, 1993; Vissers et al., 2004). CHARGE affects 1 in 8,500 to 1 in 12,000 births (Kallen et al., 1999; Issekutz et al., 2005). Partial or complete hypoplasia of the semicircular canals is present in almost all patients with CHARGE (Tellier et al., 1998), making the vestibular phenotype a reliable and consistent manifestation of CHARGE syndrome. Current diagnostic criteria for CHARGE include semicircular canal dysgenesis as a major criterion (Verloes, 2005). Highly variable penetrance of other CHARGE features has been noted, even in monozygotic twins, suggesting epigenetic influences on gene expression and/or function (Johnson et al., 2005).

Between 60 and 80% of CHARGE patients are heterozygous for *CHD7* mutations, including nonsense, deletion, and missense mutations; however, no correlations have

Grant sponsors: National Institutes of Health; Grant numbers: R01-DC01634 and P30 DC05188 (to Y.R.) and K08 HD40188 (to D.M.M.); Grant sponsor: the National Organization for Hearing Research Foundation (NOHR; to Y.R. and D.M.M.); Grant sponsor: the Williams Professorship; Grant sponsor: Berte and Alan Hirschfield; Grant sponsor: the Center for Hearing Disorders (CHD).

*Correspondence to: Donna M. Martin, 1150 W. Medical Center Dr., 3520A MSRB I, Ann Arbor, MI 48109-0652.
E-mail: donnamm@umich.edu

Received 10 March 2007; Revised 9 June 2007; Accepted 29 June 2007
DOI 10.1002/cne.21460
Published online in Wiley InterScience (www.interscience.wiley.com).

been found between specific mutations and associated phenotypes (Vissers et al., 2004; Sanlaville et al., 2005; Aramaki et al., 2006; Jongmans et al., 2006; Lalani et al., 2006). Human *CHD7*, located on chromosome 8q12.1, is a member of the family of chromodomain helicase DNA-binding genes, which code for proteins that are presumed to affect chromatin structure and gene expression (Woodage et al., 1997). The CHD7 protein may regulate expression of genes that are essential for development of the inner ear and other CHARGE-affected tissues (Bosman et al., 2005; Lalani et al., 2006).

We have established a mouse model for CHARGE that enables us to study vestibular development, pathology, and potential for future interventions (Hurd et al., 2007). Heterozygous $Chd7^{Gt/+}$ mice were generated from gene-trapped embryonic stem cells containing a β-galactosidase reporter cassette (Hurd et al., 2007). Heterozygous $Chd7^{Gt/+}$ and other *Chd7*-deficient mice are a good model of CHARGE syndrome, because they exhibit semicircular canal defects, circling behaviors, variable hearing loss, and increased numbers of hair cells in the organ of Corti, whereas homozygous $Chd7^{Gt/Gt}$ mice are embryonic lethal (Kiernana et al., 2002; Bosman et al., 2005; Hurd et al., 2007). Mature inner ear phenotypes in *Chd7*-deficient mice are less well understood, and there is no information about the structure and function of vestibular epithelia and innervation with *Chd7* deficiency.

The inner ear is a complex organ responsible for hearing and balance. The sensory epithelium and the primary neurons for hearing and balance develop from an ectodermally derived placode that forms the otocyst (Fritzsch et al., 2005). A series of invaginations, fusion events, and differential growth activities lead to the formation of the hearing organ (cochlea) and balance organs (vestibular system) (Fekete, 1996). The vestibular system is comprised of five sensory patches: the maculae of the saccule and utricle and one crista ampullaris for each of the three semicircular canals (anterior, posterior, and lateral) (Barald and Kelley, 2004; Desai et al., 2005a,b). The saccule and utricle perceive linear acceleration through a patch of sensory epithelium called the macula (Desai et al., 2005b). Each of the three semicircular canals perceives angular acceleration through a sensory patch called the crista ampullaris. Together, they function to maintain head position and balance.

At one end of each canal, a bulbous cavity called the ampulla becomes visible by embryonic day 15 in mice (Morsli et al., 1998). Each of the three ampullae contains a sensory epithelium organ called a crista ampullaris, which contains sensory hair cells that connect with vestibular nerve endings (Goldberg et al., 1985; Desai et al., 2005a). All five vestibular sensory epithelia consist of a mosaic of mechanosensory hair cells and non-sensory supporting cells. Each crista is found in a bulbous expansion that becomes visible at one end of the canal by embryonic day 15 in the mouse.

Here we report the results of an extensive evaluation of mature $Chd7^{Gt/+}$ inner ears. We observed several abnormalities in the gross morphology of $Chd7^{Gt/+}$ semicircular canals and in the vestibular sensory epithelia and their innervation. These data indicate a requirement for *Chd7* in vestibular development and innervation, with important consequences for designing rational therapies for CHARGE-related balance disorders.

Abbreviations

a	anterior
aa	anterior ampulla
ac	anterior canal
acr	anterior crista ampullaris
bb	bird-beak deformity
cc	common crus
co	cochlea
cr	crista ampullaris
d	dorsal
ec	epithelial connection (of bird-beak)
ed	endolymphatic duct
l	lateral
la	lateral ampulla
lc	lateral canal
lcr	lateral crista ampullaris
lt	lateral canal truncation
m	medial
ow	oval window
p	posterior
pa	posterior ampulla
pc	posterior canal
pcr	posterior crista ampullaris
sc	septum cruciatum
ut	utricle
v	vestibule
vn	vestibular nerve

MATERIALS AND METHODS

Mice

$Chd7^{Gt/+}$ mice were generated and characterized as previously described (Hurd et al., 2007). *Chd7* mutant (*Gt*) and wildtype alleles were also genotyped as previously described (Hurd et al., 2007). Mice were maintained by backcrossing with C57BL/6J mice (Jackson Laboratory, Bar Harbor, ME) or 129S1/SvImJ mice (Jackson Laboratory) to generation N2. Mice analyzed were male or female adults, ranging from 3 weeks to 11 months in age. All procedures were approved by The University of Michigan University Committee on Use and Care of Animals (UCUCA).

$Chd7^{Gt/+}$ (n = 25) and wildtype (n = 8) littermate mice were studied. Gross morphologic examination was performed on all ears. Among these mice, 19 $Chd7^{Gt/+}$ mice and four littermate wildtype mice were designated for epifluorescence analysis; 6 $Chd7^{Gt/+}$ mice and three littermate wildtype mice were designated for electron microscopy analysis. Mice from the entire range of ages (3 weeks to 11 months) were used for each of the analyses and were found to have similar morphologies, indicating that no obvious developmental or aging changes occurred within this age range.

Dye filling of inner ears

Mice were anesthetized with a mixture of xylazine (0.0024 mg/g) and ketamine (0.012 mg/g) and then decapitated. Temporal bones were removed and fixed locally by opening the oval and round windows, opening a perforation in the apical end of the cochlea, and gently perfusing 4% paraformaldehyde. Once fixed, ears designated for epifluorescence were instilled with fast green dye (100 mg in 10 ml phosphate-buffered saline [PBS]; Sigma, St. Louis, MO) through the oval window with a microcanula connected to a 1-ml syringe. Once filled with dye, ears were observed and photographed on a Leica MZ-12 stereomi-

croscope with a digital SPOT Insight QE camera. Once dye distribution in the inner ear was recorded, the bone was dissected away to expose the membranous labyrinth and surrounding soft tissues. The dye appeared to fill both the endolymphatic and perilymphatic fluid spaces of the inner ear, likely due to ruptured membranes that resulted in connections between the two spaces. Ears that were dye-filled were further used for epifluorescence as described below. No dye filling was performed on ears designated for electron microscopy.

Epifluorescence analysis of vestibular sensory epithelia

Tissues were permeabilized with 0.3% Triton X-100 in PBS (pH 7.3-7.4) for five minutes. After rinsing in PBS, they were treated with Image-iT® FX signal enhancer (Invitrogen, Carlsbad, CA) for 30 minutes. After additional rinsing, some specimens were blocked in normal goat serum (1%) and bovine serum albumin (0.1%) for 30 minutes. To label 200-kDa neurofilament, tissues were incubated for 1 hour in monoclonal mouse anti-neurofilament 200 antibody (Sigma, no. N0142) diluted 1:50. The carboxyterminal tail segment of enzymatically dephosphorylated pig neurofilament H-subunit was used as the immunogen. This antibody localizes in neurofilaments of molecular weight 200 kDa in rat spinal cord extract by immunoblotting (manufacturer's technical information). The pattern of anti-neurofilament staining in our study is similar to that previously reported with other anti-neurofilament antibodies in inner ear neurons (Dau and Wenthold, 1989; Berglund and Ryugo, 1991).

After rinsing, the tissues were incubated for 30 minutes with rhodamine-conjugated goat anti-mouse secondary antibody (Jackson Immunochemicals, West Grove, PA, code no. 115-025-146, lot # 61962) diluted 1:200. To label F-actin, Alexa Fluor 488-conjugated phalloidin (Invitrogen, cat. no. A12379) diluted 1:300 was added to the secondary antibody. Phalloidin labels actin, which is abundant in stereocilia and cell junctions, and enhances identification of cell types in the sensory epithelium (Meiteles and Raphael, 1994; Raphael et al., 1994). Tissues were mounted on microscope slides with ProLong Gold Antifade (Invitrogen). Tissue analysis and epifluorescence photomicroscopy were performed on a Leica DMRB microscope with 40× and 100× objective lenses.

Scanning electron microscopy (SEM)

For SEM analysis, temporal bones were removed, the cochleae were exposed, and the samples were fixed in 3% glutaraldehyde, 2% paraformaldehyde, 1% acrolein in 0.1 M cacodylate buffer (pH 7.2–7.4) (Osborne and Comis, 1991). Tissues were processed by using the OTOTO method (Osborne et al., 1984). Samples were dehydrated in increasing concentrations of ethanol and critical point dried with CO_2 in a SamDri 790 (Tousmis, Rockville, MD). Samples were examined on an Amray 100B microscope and photographed digitally. Adobe (San Jose, CA) Photoshop 9.0 was used to colorize and merge immunofluorescence images and to adjust contrast, brightness, size, and sharpness of all images.

RESULTS

Chd7$^{Gt/+}$ mice exhibit circling behaviors, embryonic semicircular canal defects, and β-galactosidase reporter expression in CHARGE-relevant tissues; homozygous *Chd7*$^{Gt/Gt}$ embryos do not survive beyond embryonic day 10.5 (Hurd et al., 2007). A full description of the *Chd7*$^{Gt/+}$ mouse is provided elsewhere (Hurd et al., 2007). Briefly, the *Chd7*^{Gt} allele contains retroviral vector sequences upstream of the ATG-containing exon 2 of *Chd7*. This abolishes proper splicing between exons 1 and 2 and is predicted to disrupt normal CHD7 protein because the mutant allele lacks upstream sequences necessary for ribosomal entry and translation. Phenotypes of *Chd7*$^{Gt/+}$ mice resemble other heterozygous *Chd7*-deficient mice (Bosman et al., 2005), demonstrating that they are a good model of CHARGE syndrome.

Variable defects in lateral and posterior semicircular canals of *Chd7*$^{Gt/+}$ mice

For a full description of normal inner ear morphology including the types of hair cells, innervation, and ampulla and canal morphology, we refer the reader to Desai et al. (2005a,b) and Goldberg et al. (1990). The overall morphology of the bony and membranous labyrinths from right and left ears of *Chd7*$^{Gt/+}$ mice (n = 50 ears) and wildtype littermates (n = 16 ears) was examined stereoscopically. All wildtype mice had normal inner ear morphology, as detailed in Figure 1A,B (see list of abbreviations). Inner ears were injected with fast green dye through the oval window. The fluid spaces in the normal inner ear are continuous through the cochlea and the three semicircular canals that open into the vestibule. One end of each canal widens to form the ampulla. The non-ampullated end of the lateral canal opens directly into the vestibule. The non-ampullated ends of the anterior and posterior canals join to form the common crus before entering the vestibule. The anterior semicircular canal and its corresponding ampulla were present in all *Chd7*$^{Gt/+}$ ears and appeared normal.

Abnormalities of lateral canal morphology were observed in all *Chd7*$^{Gt/+}$ inner ears examined (n = 50; Table 1). Defects ranged in severity from mild alteration of canal shape to complete truncation. In some mice, the lateral canals were truncated (Fig. 1C), and others appeared as complete, patent loops with a smaller diameter, leading to a more circular morphology compared with wildtype ("loop" canal, n = 18/50; Fig. 1D–F). Marked variability was observed in the diameter of the arc of the canal and of the canal lumen in these ears. Other lateral canals were found to have a point of luminal narrowing along their arcs, which, on dye filling, resembled a bird's beak ("bird-beak" canal, n = 13/50; Fig. 1F–H,J). Most commonly, the beak was noted at the non-ampullated end of the canal, just proximal to its opening into the vestibule, although occasionally it was found near the midsection of the canal or, in two ears, near the ampullated end. The constriction was mild in some ears, but in others, the connection between the non-ampullated end and the vestibule was narrow and could be confirmed only by dye instillation (Fig. 1G) and/or epithelial dissection (Fig. 1H,J).

The most severe lateral canal defect observed in *Chd7*$^{Gt/+}$ mice was the complete truncation of the non-ampullated end (n = 19/50; Fig. 1C,I). The length of the canal proximal to the truncation varied from greater than half of the usual canal circumference to no more than a tiny bud off the ampulla. On epithelial dissection, the lateral ampulla was present in most ears. In four of 50 *Chd7*$^{Gt/+}$ ears, both the ampulla and corresponding crista

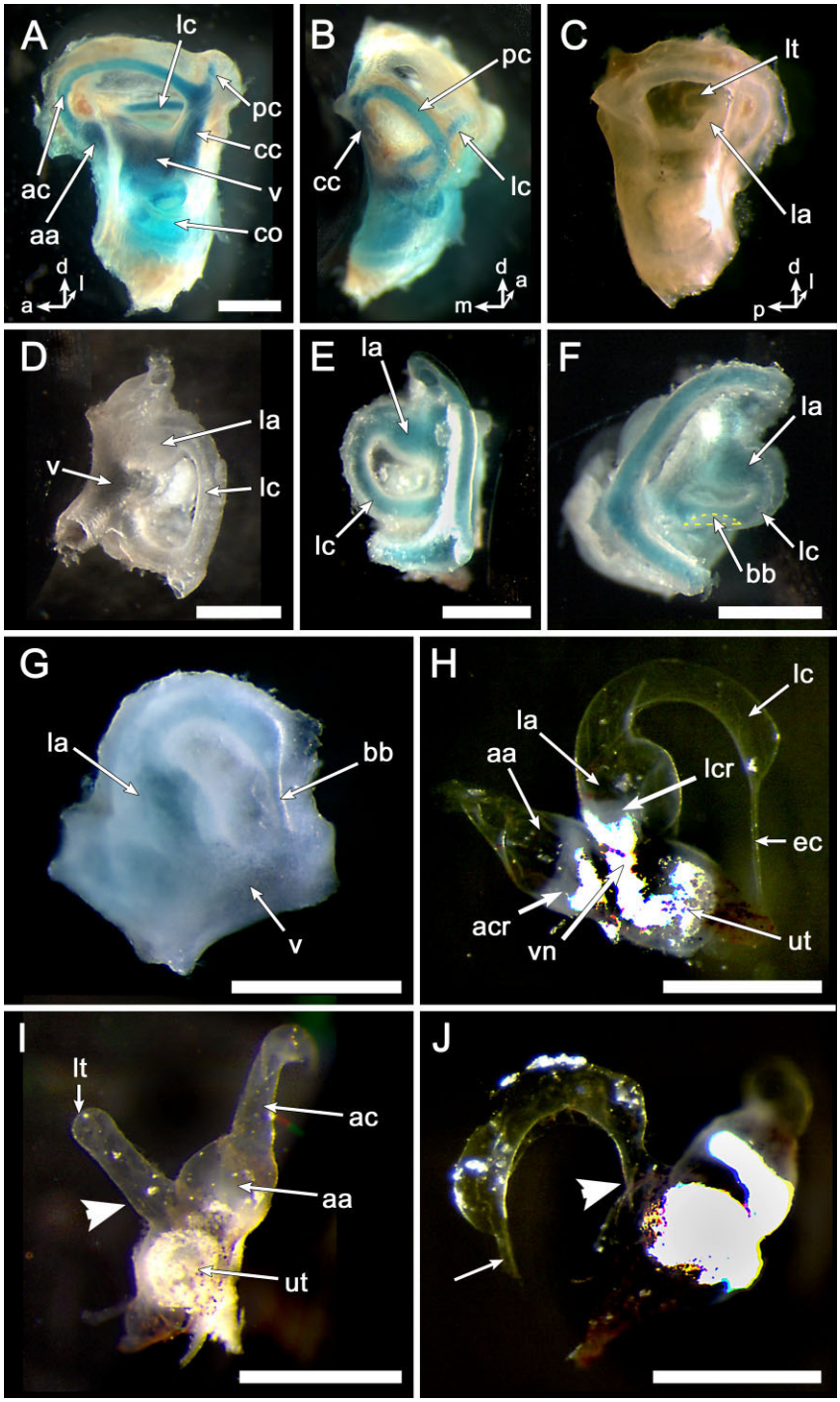

Fig. 1. Lateral canal defects in *Chd7*$^{Gt/+}$ inner ears. Stereoscopic images of the vestibular portion of inner ears from wildtype (A,B,D) and mutant *Chd7*$^{Gt/+}$ (C,E–J) mice. **A,B:** Fast green dye-filled right ear from a 21-day-old wildtype mouse, with the ventral aspect pointing down and anterior to left (A) or back (B). The anterior canal (ac) is round and has one ampullated end (aa). The non-ampullated end of the anterior canal meets the oval-shaped posterior canal (pc) to jointly form the common crus (cc). Part of the lateral canal (lc) is visible. The lateral canal enters directly into the vestibule (v). **C:** The lateral canal in a left *Chd7*$^{Gt/+}$ ear, before dye-filling, is truncated (lt) at the midpoint of the canal arc, at the non-ampullated end. **D:** An elliptical-shaped wildtype right lateral canal within its bony capsule, before dye-filling. **E:** A loop-shaped lateral canal from a left *Chd7*$^{Gt/+}$ ear is smaller and more circular than in wildtype (D). **F:** The lateral canal from a right *Chd7*$^{Gt/+}$ ear demonstrates a bird-beak (bb) deformity, with a narrowing of the canal lumen near the non-ampullated end. **G:** A severe right bird-beak lateral *Chd7*$^{Gt/+}$ canal tapers toward the vestibule, such that dye barely penetrates the narrowing membranous vestibular tissues. **H:** After bone removal from the canal in G, a thin epithelial connection (ec) is seen between the end of the canal and the vestibule (v). The lateral (lcr), anterior cristae (acr), utricle (ut), and corresponding vestibular nerve bundles (vn) are seen. **I:** In the left *Chd7*$^{Gt/+}$ ear, the lateral ampulla is absent (arrowhead) and the lateral canal is truncated (lt). **J:** In another left *Chd7*$^{Gt/+}$ ear, the lateral ampulla is absent and is replaced by a narrow epithelial lumen (arrowhead). The membranous connection between the bird-beak deformity and the vestibule is present at the other end of the canal epithelium (white arrow). Scale bar = 1 mm in A (applies to A–C) and D–J.

TABLE 1. SUMMARY OF SEMICIRCULAR CANAL AND SENSORY EPITHELIAL DEFECTS IN *CHD7*$^{GT/+}$ MUTANT MICE

	Semicircular canal morphology						Sensory epithelial defects				
Mouse no.	Circler (Y/N)	L/R	Lateral	Post	Ant	Tech. used	Lateral	Posterior morphology	Posterior innervation	Utricle	Saccule
1	Y	R	trunc	pres	nl	SEM	nl	—	—	nl	nl
		L	trunc	pres	nl	—	—	—	—	—	—
2	Y	R	trunc	pres	nl	—	—	—	—	—	—
		L	trunc	pres	nl	SEM	nl	saddle; rud. septum	—	nl	nl
3	Y	R	trunc	pres	nl	—	—	—	—	—	—
		L	trunc	abs	nl	—	—	—	—	—	—
4	Y	R	trunc	abs	nl	—	—	—	—	—	—
		L	trunc	abs	nl	IF	nl	patch; no septum	abs	nl	nl
5	Y	R	trunc	pres	nl	IF	nl	saddle; rud. septum	abs	nl	—
		L	trunc	pres	nl	IF	no amp.	saddle; rud. septum	abs	nl	—
6	Y	R	trunc	pres	nl	IF	nl	—	abs	nl	—
		L	trunc	abs	nl	—	no amp.	—	—	—	—
7	Y	R	trunc	pres	nl	IF	nl	saddle; rud. septum	red.	nl	nl
		L	bird—beak	pres	nl	IF	—	saddle; nl septum	pres	—	—
8	Y	R	bird—beak	pres	nl	IF	—	saddle; nl septum	abs	nl	—
		L	trunc	pres	nl	IF	—	—	—	nl	nl
9	Y	R	bird—beak	pres	nl	SEM	nl	saddle; rud. septum	—	—	—
		L	bird—beak	pres	nl	—	no amp.	—	—	—	—
10	N	R	trunc	pres	nl	IF	nl	patch; no septum	abs	nl	—
		L	trunc	pres	nl	IF	nl	—	—	—	—
11	N	R	trunc	pres	nl	IF	nl	saddle; nl septum	abs	nl	nl
		L	bird—beak	abs	nl	IF	nl	—	abs	—	—
12	N	R	bird—beak	abs	nl	IF	nl	patch; rud. septum	abs	nl	—
		L	bird—beak	pres	nl	IF	nl	saddle; rud. septum	abs	nl	—
13	N	R	trunc	pres	nl	IF	—	saddle; rud. septum	pres	nl	—
		L	loop	pres	nl	IF	nl	saddle; rud. septum	abs	nl	—
14	N	R	loop	pres	nl	IF	nl	saddle; rud. septum	abs	nl	—
		L	trunc	pres	nl	IF	nl	saddle; rud. septum	pres	nl	—
15	N	R	bird—beak	pres	nl	IF	nl	—	—	nl	—
		L	loop	pres	nl	IF	nl	saddle; nl septum	abs	nl	—
16	N	R	bird—beak	pres	nl	IF	nl	saddle; rud. septum	abs	—	nl
		L	loop	pres	nl	IF	—	saddle; rud. septum	abs	nl	nl
17	N	R	loop	pres	nl	IF	nl	saddle; rud. septum	abs	nl	—
		L	bird—beak	pres	nl	IF	—	saddle; rud. septum	abs	—	—
18	N	R	bird—beak	pres	nl	IF	nl	saddle; rud. septum	pres	nl	—
		L	loop	pres	nl	IF	nl	saddle; rud. septum	abs	—	—
19	N	R	loop	pres	nl	SEM	nl	—	—	—	—
		L	bird—beak	pres	nl	SEM	nl	—	—	—	—
20	N	R	bird—beak	pres	nl	SEM	nl	—	—	—	—
		L	loop	pres	nl	SEM	nl	saddle; nl septum	—	—	—
21	N	R	loop	pres	nl	SEM	sm. patch	—	—	nl	nl
		L	loop	pres	nl	—	—	—	—	—	—
22	N	R	loop	pres	nl	—	—	—	—	—	—
		L	loop	pres	nl	—	—	—	—	—	—
23	N	R	loop	pres	nl	IF	—	—	—	—	nl
		L	loop	pres	nl	IF	—	—	—	nl	—
24	N	R	loop	pres	nl	IF	nl	saddle; rud. septum	pres	nl	nl
		L	loop	abs	nl	IF	nl	saddle; rud. septum	pres	nl	—
25	N	R	loop	pres	nl	—	—	—	—	—	—
		L	loop	abs	nl	IF	no amp.	saddle; rud. septum	pres	nl	nl

Abbreviations: abs, absent; amp., ampulla; IF, immunofluorescence; —, not done; nl, normal; L, left ear; pres, present; rud., rudimentary; R, right ear; SEM, scanning electron microscopy; sm., small; trunc, truncation; red, reduced.

were absent (Fig. 1I,J). Of the four *Chd7*$^{Gt/+}$ ears missing the lateral ampulla, the lateral semicircular canal formed a complete but smaller loop in one ear, a bird-beak in another ear, and was truncated in the other two ears.

Variability in lateral semicircular canal defects was frequently observed not only between different *Chd7*$^{Gt/+}$ mice but also between the right and left ears of the same mouse (Tables 1, 2). Of the 13 mice with at least one loop deformity of the lateral canal, 5 had bilateral loops, 6 had a bird-beak deformity of the contralateral canal, and 2 had a contralateral lateral canal truncation. Variability in loop size was often noted between the ears of mice with bilateral loops. Of the 12 mice with at least one lateral canal truncation, 7 had bilateral truncations, 3 had a contralateral bird-beak, and 2 had a contralateral loop. The extent of lateral canal truncation also varied between ears in some mice. The intra-animal variability was higher for the beak morphology than for the loop and truncated lateral canals. Only 2 of the 11 mice with at least one beak had bilateral beaks. Again, the site and degree of narrowing was not identical between the ears of those mice with bilateral beaks. No mice were missing the lateral ampulla in both ears. In total, 14/25 mice had similar, though not necessarily identical, malformations of the lateral canal between ears, and 11/25 had different malformations of the lateral canal between ears.

TABLE 2. Correlations Between Lateral Semicircular Defects and Circling Behaviors in *Chd7*$^{Gt/+}$ Mice

Lateral semicircular canal morphology	No. of circlers	No. of non-circlers	Total no. of mice
Bilateral truncation	6	1	7
Truncation with contralateral bird-beak	2	1	3
Bilateral bird-beak	1	1	2
Truncation with contralateral loop	0	2	2
Bird-beak with contralateral loop	0	6	6
Bilateral loop	0	5	5
Total no. of mice	9	16	25

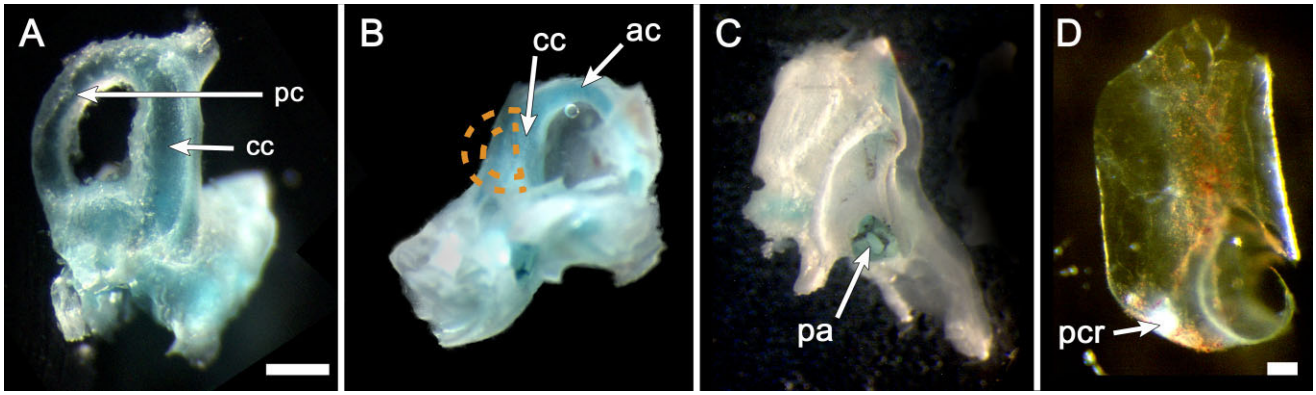

Fig. 2. Posterior canal defects in *Chd7*$^{Gt/+}$ inner ears. **A:** Isolated posterior canal of a left *Chd7*$^{Gt/+}$ ear showing a D-shaped canal with a smaller canal arc diameter, shorter common crus, and wider canal lumen diameter compared with the oblique ellipse in the wildtype (see Fig. 1B). **B:** In some *Chd7*$^{Gt/+}$ ears, the posterior canal is missing (dashed line), and the common crus (cc) appears wider. **C:** With the bony covering of the common crus removed, the membranous part of the crus encloses an expanded cavity (dashed line) with the posterior ampulla (pa) located at the ventral aspect of the common cavity. **D:** Removal of bone from the dashed area in C reveals the posterior crista (pcr) and the enlarged common crus (cc) lumen. For other abbreviations, see list. Scale bar = 1 mm in A (applies to A–C); 0.2 mm in D.

We also noted dysplasia of the posterior canal in *Chd7*$^{Gt/+}$ mice. A complete posterior canal was present in the majority of *Chd7*$^{Gt/+}$ ears (n = 42/50); however, the morphology varied from that of wildtype littermates. Due to the small size and irregular surfaces of the specimens, it was difficult to orient the posterior canal properly to take accurate measurements of the canal size. Subjectively, the canal arc diameter appeared smaller, the canal lumen wider, and the common crus shorter, such that the canal assumed a more circular, D shape (Fig. 2A), rather than the oblique elliptical shape noted in wildtype ears (Fig. 1B). In a few ears, the superior aspect of the posterior canal joined the vertical portion of the anterior canal farther along its course, leading to an even smaller canal arc (data not shown). A distinct posterior canal was absent in a smaller proportion of the ears (n = 8/50 ears, in 7/25 mice). In these cases, the morphology of the common crus was altered. In some of these ears, the area of the common crus formed a markedly widened bony cavity that, on epithelial dissection, was found to contain a patulous common epithelial lumen (Fig. 2B–D). In other cases, it appeared as a cavity of almost normal width, associated with a small, truncated out-pouching from the superior end, where the posterior canal would otherwise be (n = 2/8, not shown). On gross observation during dissection, the posterior crista was always present within the bony posterior ampulla, regardless of the presence of a distinct posterior canal (n = 50/50; Fig. 2D). The size and shape of the posterior canal often varied between ears of the same animal and was bilaterally absent in only one of the seven mice with absence of a distinct posterior canal (Table 1).

Sensory epithelium abnormalities in *Chd7*$^{Gt/+}$ mice

Following stereoscopic examination, the three cristae and the utricular and saccular maculae from *Chd7*$^{Gt/+}$ (n = 31) and wildtype littermate (n = 7) ears were stained for actin and neurofilament and viewed as whole mounts with epifluorescence. This preparation method allows for detailed analysis of the entire sensory epithelium. Stereocilia and cell adherens junctions contain actin filaments, so actin was used as a marker to delineate surface morphology, cell borders, and stereocilia presence and configuration. Similarly, neurofilament staining was used to define the nerve fibers and terminal calyces that surround the flask-shaped, type I vestibular sensory cells in each organ. Axons of the vestibular branch of the eighth cranial nerve form calyces around type I hair cells and button-type terminals at the basal end of type II hair cells (Goldberg et al., 1985; Desai et al., 2005a,b). Due to the challenging nature of the tissue preparation, not all five sensory organs were preserved in every specimen (Table 1).

Each of the five vestibular organs exhibited sensory cells with intact stereocilia organized in a step-like fashion, surrounded by supporting cells (Fig. 3). Like its corresponding anterior ampulla, the anterior crista was present in all *Chd7*$^{Gt/+}$ (n = 27) and wildtype (n = 5) ears examined (Fig. 3). The anterior cristae of both *Chd7*$^{Gt/+}$ and wildtype mice assumed a typical saddle shape and were comprised of sensory cells with a normal stereocilia bundle configuration (Fig. 3). In both *Chd7*$^{Gt/+}$ and wildtype mice, the sensory epithelium was completely divided at its midpoint by a non-sensory area, the septum cruciatum, which is characteristic of murine anterior and posterior cristae (Fig. 3A,D). On stereoscopic brightfield inspection, a dense white nerve bundle was observed to enter the anterior crista on the undersurface of both *Chd7*$^{Gt/+}$ and wildtype ears (Fig. 1H and data not shown). Neurofilament staining of *Chd7*$^{Gt/+}$ and wildtype ears demonstrated a dense array of calyx-shaped nerve terminals that surrounded the cell bodies of stereocilia-bearing sensory cells (Fig. 3B,E).

In deeper planes of the crista, the nerve terminals could be traced back toward branch points and common nerve fibers (data not shown). An area of dense neurofilament staining was noted in *Chd7*$^{Gt/+}$ and wildtype ears at the mid-portion of the septum cruciatum (Fig. 3E,F); a similarly dense area was noted when the deepest, most central portions of the cristae beneath the stereocilia-bearing surface were examined (data not shown). The anterior cristae of *Chd7*$^{Gt/+}$mice resembled those of wildtype mice in surface morphology and innervation pattern. Subjectively,

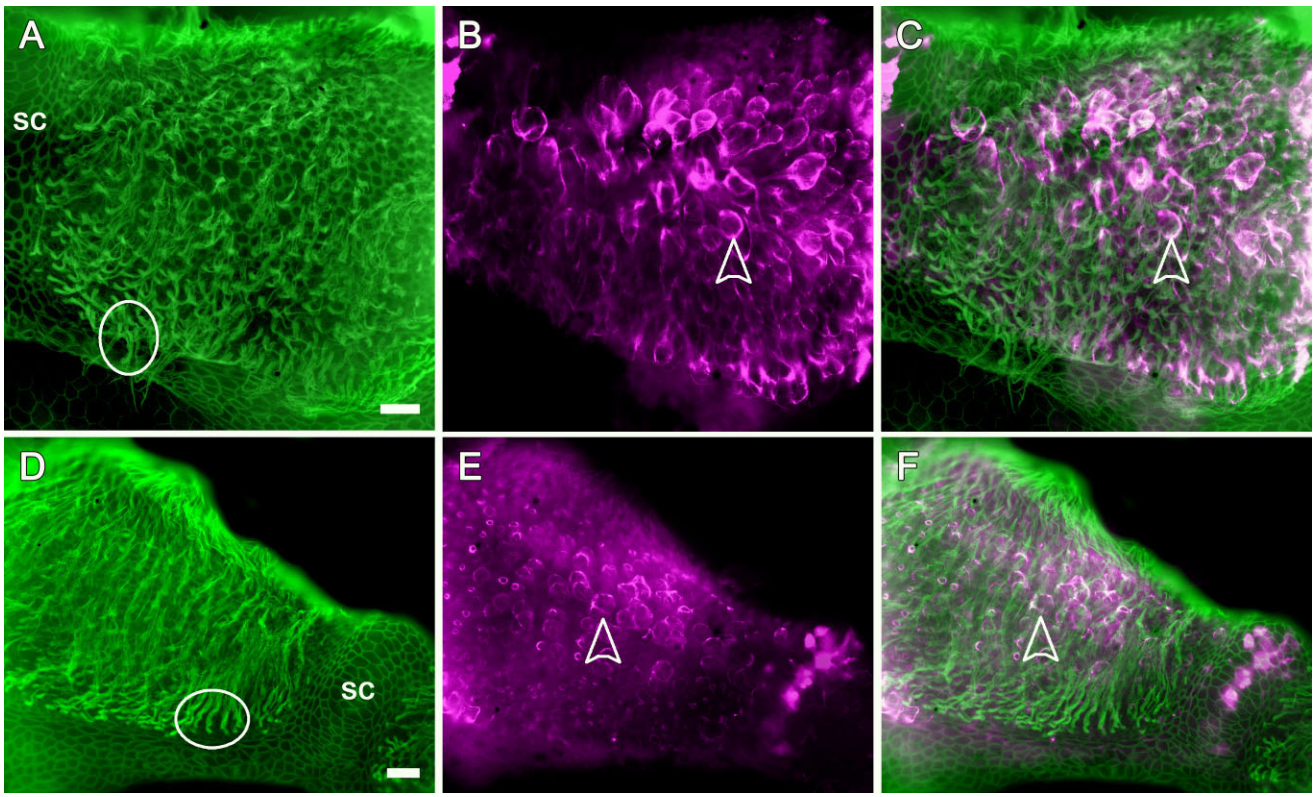

Fig. 3. Normal anterior crista ampullaris in $Chd7^{Gt/+}$ mice. Epifluorescence images of whole mounts of the anterior crista ampullaris showing the central part (septum cruciatum; sc in A and D) and one side of the anterior crista of wildtype (**A–C**) or $Chd7^{Gt/+}$ (**D–F**) ears stained for actin (A,D) and neurofilament (B,E) with merged images shown in C and F. The wildtype sensory epithelium is densely populated with hair cells that exhibit tall stereocilia (circled areas in A,D). The septum cruciatum (sc in A,D) in the central area of the sensory epithelium is devoid of hair cells. Nerve fibers and chalice-shaped nerve terminals (arrowheads in B,E) densely populate the sensory epithelium. Merged image shows nerve calyces surrounding hair cells (arrowheads in C,F). Scale bar = 20 μm in A (applies to A–C) and D (applies to D–F).

they appeared to be of similar size, but this was not measured.

The lateral crista ampullaris was present in all wildtype ears and in all $Chd7^{Gt/+}$ ears that had a lateral ampulla (n = 21 $Chd7^{Gt/+}$; n = 8 wildtype ears; Fig. 4). No lateral sensory epithelium was present in the four $Chd7^{Gt/+}$ ears lacking a lateral ampulla. The shape, surface morphology, and neurofilament staining pattern of lateral cristae from $Chd7^{Gt/+}$ mice resembled those in wildtype ears (Fig. 4). Unlike posterior and anterior cristae, lateral cristae of the wildtype lack a septum cruciatum. All $Chd7^{Gt/+}$ ears also lacked a septum cruciatum, but one ear did have a small, hair cell-free patch in the lateral crista ampullaris reminiscent of a septum cruciatum. This may be a rare variant of unclear significance. On high-magnification view, the $Chd7^{Gt/+}$ lateral crista hair cell bundle configuration was normal,and nerve calyces were clearly associated with sensory cells (Fig. 4C,F). The width of the lateral crista in some $Chd7^{Gt/+}$ ears appeared smaller than in wildtype ears on both stereoscopic examination of epithelium and on whole mount preparation, and the vestibular nerve bundle entering the crista was visibly smaller than wildtype on stereoscopy. These findings were present independent of the degree of severity of the lateral canal dysplasia.

By immunofluorescence, the posterior crista ampullaris was present in all $Chd7^{Gt/+}$ (n = 26) and wildtype (n = 8) ears examined, and abnormalities of the morphology and/or innervation of the posterior crista ampullaris were noted in all 26 $Chd7^{Gt/+}$ ears. The morphologic defects ranged from an apparent reduction in the surface area of the saddle-shaped sensory epithelium to a flattening of the saddle into a round, patch-like epithelium (Fig. 5). The posterior septum cruciatum appeared normal in three $Chd7^{Gt/+}$ ears and was absent in two $Chd7^{Gt/+}$ ears, both of which had a small, patch-like sensory epithelium (Fig. 5). The other 21 $Chd7^{Gt/+}$ ears had a small area devoid of stereocilia at the edge of the sensory epithelium, which resembled a rudimentary septum cruciatum (Fig. 5K). This area was located near the center of the crista. In most instances, only one such area was present. When two hair cell-free patches were present, the areas were located on opposite (paramedial) positions in the crista. On high magnification of these ears, the hair cell bundle configuration and orientation appeared normal (data not shown).

Posterior cristae from $Chd7^{Gt/+}$ mice also displayed abnormalities in neurofilament staining. There was no evidence of any labeling of the terminal nerve calyces or axons in the majority of the $Chd7^{Gt/+}$ posterior cristae (n = 18/26; Fig. 5). In this group of ears, when a complete or rudimentary septum cruciatum was present, the typically dense neurofilament staining was still noted in the plane beneath the epithelial surface in this region (Fig. 5). The remaining cristae demonstrated some terminal caly-

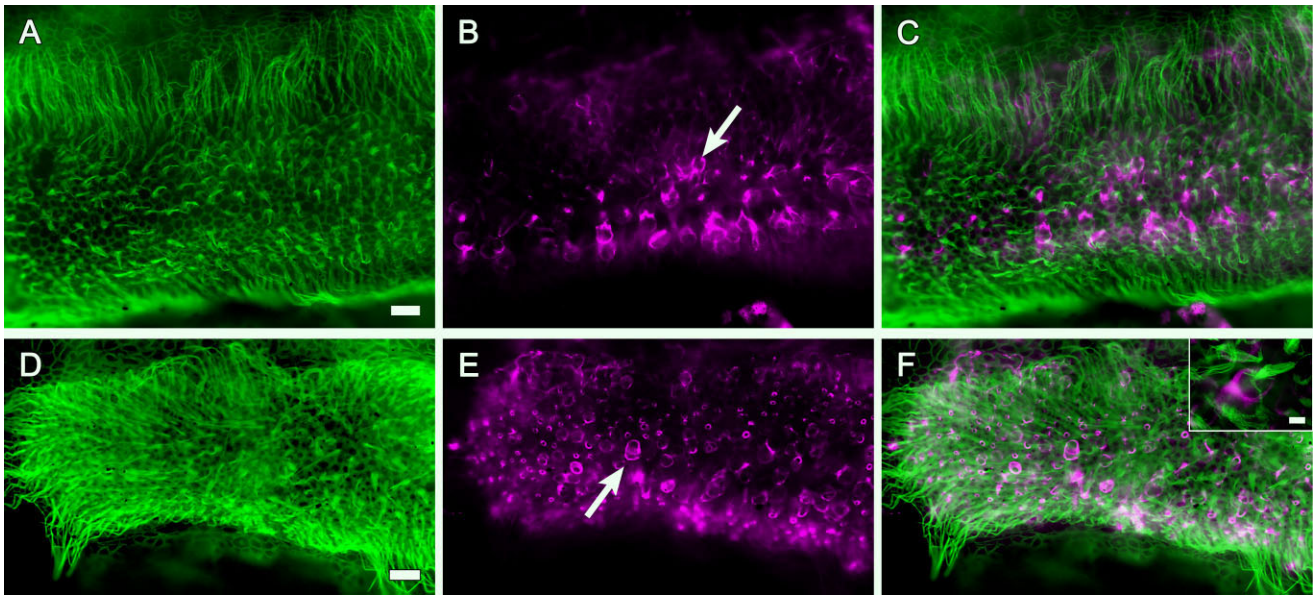

Fig. 4. Normal lateral crista ampullaris in *Chd7*$^{Gt/+}$ mice. Epifluorescence images of the central portion of the lateral cristae of wildtype (**A–C**) or *Chd7*$^{Gt/+}$ mutants (**D–F**) stained for actin (A,D) and neurofilament (B,E) with merged images shown in C and F. The wildtype and *Chd7*$^{Gt/+}$ lateral cristae lack a septum cruciatum and have hair cells with tall stereocilia (A,D). The *Chd7*$^{Gt/+}$ crista is visibly smaller (compare D with A). A dense array of nerve calyces underlies the epithelial surface in both wildtype and *Chd7*$^{Gt/+}$ ears (representative calyces indicated by arrows in B,E). Merged images show calyces surrounding hair cells (C,F). In the high-magnification inset in F, the close relationship between the hair cell and nerve calyx is notable. Scale bar = 20 μm in A (applies to A–C) and D (applies to D–F); 10 μm in inset to F.

ces, ranging in density from a few cups per crista (right ear from mouse no. 7, Table 1) to the typical even distribution of cups throughout the crista (Fig. 5; n = 7/26). Absence of nerve calyces was observed in all cristae with patch-like epithelia, in one with a complete septum cruciatum, and in most with rudimentary septa. A normal neurofilament staining pattern was noted in several ears (n = 6) with a rudimentary septum cruciatum as well as in one with a normal septum cruciatum (Table 1). These data suggest that the presence of a normal posterior septum cruciatum and epithelial morphology are not sufficient for posterior crista innervation, and normal innervation does not guarantee normal epithelial morphology. Also of note, a normal posterior sensory epithelium in the absence of neurofilament staining was seen in mice as old as 11 months. Absence of neurofilament staining was noted bilaterally in five mice and only unilaterally in three.

The utricle and saccule were present in all *Chd7*$^{Gt/+}$ and wildtype ears examined (utricle: n = 24 *Chd7*$^{Gt/+}$, n = 6 wildtype; saccule, n = 9 *Chd7*$^{Gt/+}$, n = 4 wildtype). The shape, hair cell morphology, and innervation pattern of the utricular and saccular maculae of *Chd7*$^{Gt/+}$ mice was indistinguishable from wildtype animals (Fig. 6; *Chd7*$^{Gt/+}$ utricle only). Otoconia appeared normal on all specimens as bright, refractile particles on stereoscopy (Fig. 1K–M). No apparent difference in utricular size was noted between wildtype and *Chd7*$^{Gt/+}$ ears. The saccule in the mouse is difficult to obtain in its entirety; thus we were unable to make general conclusions regarding saccular size.

Fine surface morphology demonstrated by SEM

Vestibular epithelia from *Chd7*$^{Gt/+}$ (n = 8) and wildtype (n = 3) ears were examined by SEM (Fig. 7). The pattern of stereocilia at the apical surface of the vestibular hair cells of all five sensory organs appeared normal in *Chd7*$^{Gt/+}$ mice. Specifically, the stereocilia bundles appeared to be organized in the typical staircase pattern. The kinocilium was consistently present and was located on the side of the bundle displaying the longest stereocilia. Hair cell density appeared similar to that of wildtype. One *Chd7*$^{Gt/+}$ lateral crista was found to have a paramedial circular patch of microvillus-bearing cells that resembled those seen in the septum cruciatum of the anterior and posterior cristae of wildtype mice (not shown).

Correlation with behavioral phenotypes

Nine of the 25 closely observed *Chd7*$^{Gt/+}$ mice had circling behaviors. Circling mice appeared to circle rapidly and bidirectionally and exhibited this behavior for much of their waking hours, although they stopped to eat, rest, and procreate. Circling behavior in mice is often considered indicative of vestibular dysfunction; thus we attempted to correlate behavioral phenotypes to the observed inner ear defects of *Chd7*$^{Gt/+}$ mice. Semicircular canal morphologies and sensory epithelial defects with associated circling behaviors are listed in Tables 1 and 2. Some lateral semicircular canal pathologies tended to be more strongly associated with circling than others. We attempted to correlate circling behaviors observed in some *Chd7*$^{Gt/+}$ mice with underlying inner ear pathologies (Tables 1, 2). All 25 mice exhibited some degree of lateral canal malformation. Only nine of these exhibited circling, and all nine had severe bilateral defects of the lateral canal (truncation or bird-beak defect on each side). Only three mice with such severe bilateral lateral canal defects were non-circlers. All 13 mice with the less severe loop defect in at least one ear were non-circlers. No circling mouse was found to have a completely patent lateral ca-

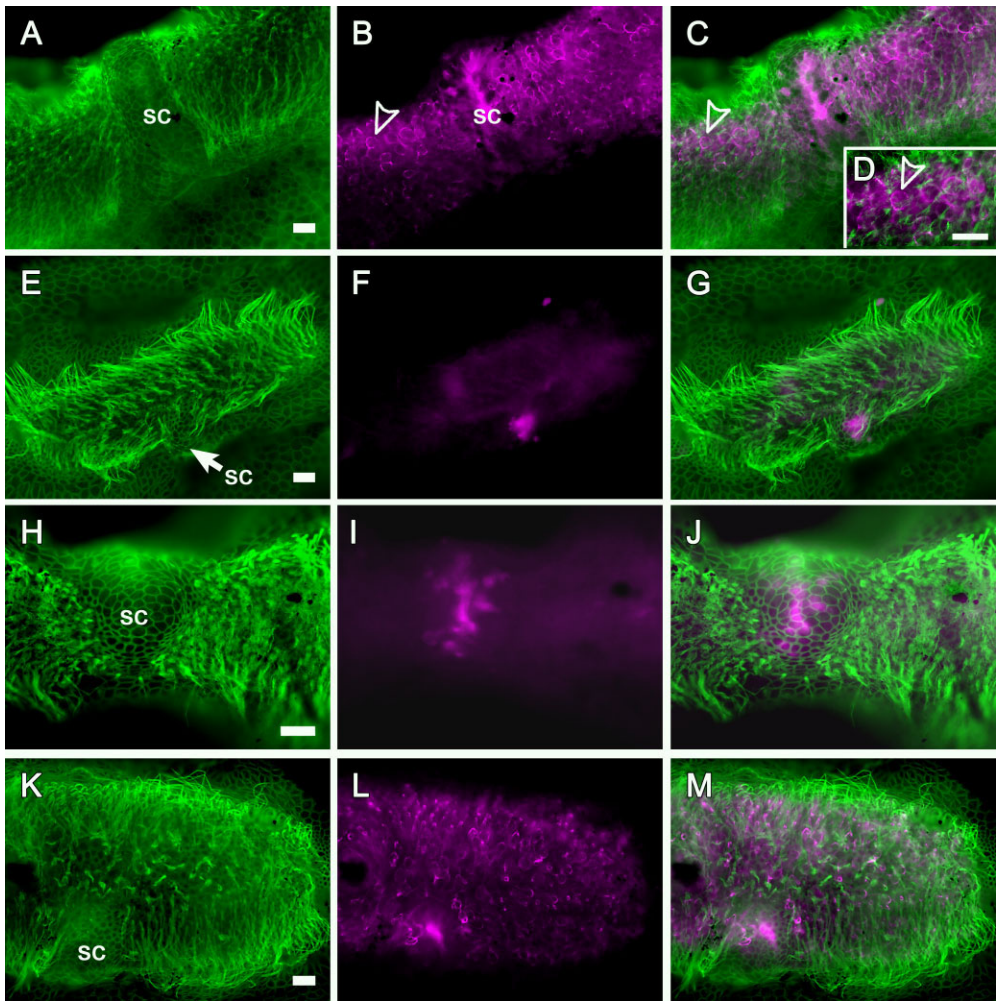

Fig. 5. Posterior crista ampullaris defects in the $Chd7^{Gt/+}$ mice. Epifluorescence images of the central portion of the posterior crista of wildtype (A–D) or $Chd7^{Gt/+}$ (E–M) ears stained for actin (A,E,H,K) and neurofilament (B,F,I,L), with merged images shown in C,D,G,J,M. **A:** The sensory epithelium is densely populated with hair cells, and the septum cruciatum (sc) is present at the center of the sensory epithelium. **B:** Terminal nerve calyces densely populate the crista (arrowhead). A dense area of neurofilament staining is seen beneath the epithelium of the septum cruciatum (sc). **C,D:** The nerve calyces surround hair cells in (arrowheads). **E,F:** Some mutant cristae (E) have hair cells with tall stereocilia, but the area of the sensory epithelium is small, the septum cruciatum (sc; arrow) is rudimentary and does not extend across the entire crista, and no nerve calyces are present (F). **G:** In the merged image, dense neurofilament staining is seen at the site of the rudimentary septum cruciatum (sc). **H:** The septum cruciatum resembles the wildtype crista in A but is wider and does not span the crista. **I,J:** No nerve calyces are present. **K–M:** A focal area of dense nerve calyx staining is present in the crista in the rudimentary septum cruciatum of the mutant crista. Scale bar = 20 μm in A (applies to A–C), E (applies to E–G), H (applies to H–J), and K (applies to K–M).

nal. Analysis of the corresponding 2 × 2 contingency table indicates that there is a strong association between circling and severe bilateral malformations of the lateral canal ($\chi^2 = 14.2$, df = 1, $P < 0.0001$). These data suggest that unimpeded fluid flow through a loop-type lateral canal may be associated with milder vestibular deficits.

We also examined whether posterior canal morphology and neurofilament staining defects were associated with circling behaviors. Of the 18 $Chd7^{Gt/+}$ mice with complete bilateral posterior canals, 6 circled and 12 did not. Of the six $Chd7^{Gt/+}$ mice in which one posterior canal was missing while the contralateral posterior canal was intact, two circled and four did not. One $Chd7^{Gt/+}$ mouse with bilateral absence of the posterior canal circled. Analysis of the 2 × 2 contingency table demonstrated that circling is not significantly associated with absence of the posterior canal ($\chi^2 = 0.198$, df = 1, $P = 0.656$); 6 of 9 circlers and 12 of 18 non-circlers had both posterior canals present. Thus, the strongest relationship observed was between circling behavior and lateral canal morphology.

Among five $Chd7^{Gt/+}$ mice with bilateral absence of neurofilament staining in the posterior crista, only one exhibited circling behavior. Lack of distal innervation of the posterior crista was not sufficient to induce circling. Unilateral absence of neurofilament staining in the posterior crista (with normal staining in the contralateral ear) was observed in three $Chd7^{Gt/+}$ non-circling mice and in no $Chd7^{Gt/+}$ mice that circled, but many contralateral ears could not be examined by immunofluorescence or were damaged during tissue processing. Finally, bilateral

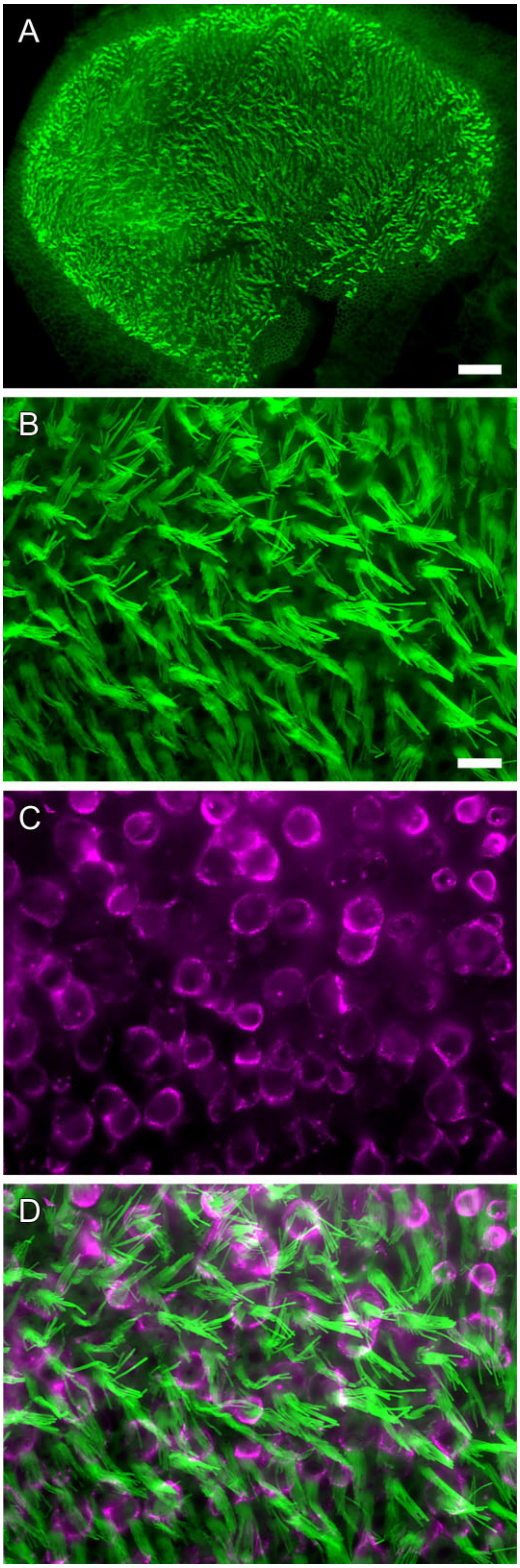

Fig. 6. Normal utricles in $Chd7^{Gt/+}$ mice. Epifluorescence images of a utricular macula of a $Chd7^{Gt/+}$ ear stained for actin (**A,B**) and neurofilament (**C**), with merged image shown in **D**. The shape of the utricle is normal and the hair cells are distributed densely and evenly throughout the sensory epithelium. Nerve calyces densely populate the macula (C) and surround the sensory cells (D). Scale bar = 50 μm in A; 10 μm in B (applies to B–D).

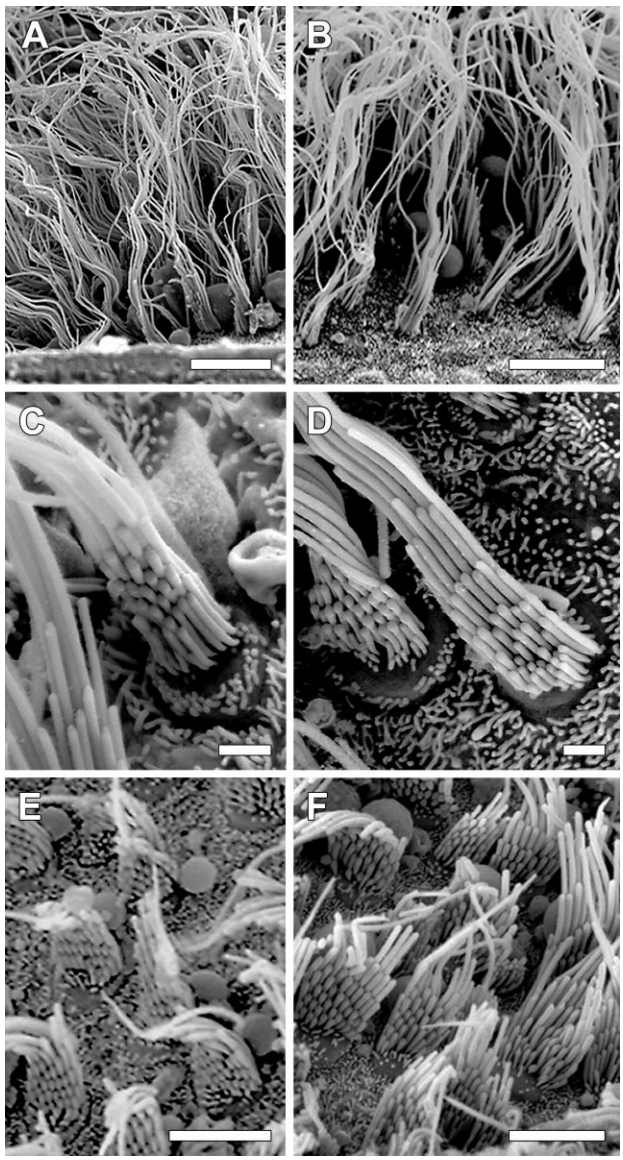

Fig. 7. Normal ultrastructural anatomy of the vestibular epithelia in $Chd7^{Gt/+}$ mice. Scanning electron micrographic images of wildtype (**A,C,E**) and $Chd7^{Gt/+}$ (**B,D,F**) vestibular epithelia. The lateral cristae of both wildtype (A) and $Chd7^{Gt/+}$ (B) ears are populated by hair cells in dense bundles, with a staircase orientation and long stereocilia on the kinocilium side. Dense bundles of stereocilia are also present in the posterior cristae of wildtype (C) and $Chd7^{Gt/+}$ (D) ears. The hair cell bundles of wildtype (E) and $Chd7^{Gt/+}$ (F) utricular maculae appear similar to each other. Scale bar = 10 μm in A,B: 1 μm in C,D; 5 μm in E,F.

nerve calyces were present in one non-circling $Chd7^{Gt/+}$ mouse and in one circling $Chd7^{Gt/+}$ mouse. Of note, the pattern of staining was asymmetric in the circling $Chd7^{Gt/+}$ mouse, with normal calyx density in one crista and sparse calyces in the other. Collectively, these data do not provide sufficient evidence for a link between the various combinations of posterior canal dysmorphologies or sensory epithelial defects and circling behavior.

DISCUSSION

The results of our experiments demonstrate severe and variable sensory epithelial defects in the vestibular system of mice with *Chd7* deficiency. These defects include abnormalities in vestibular sensory epithelial innervation and are associated with structural defects in the lateral and posterior semicircular canals.

Hair cells and innervation

Balance disorders in humans and mice can occur due to abnormal development, loss, or dysfunction of vestibular hair cells, or they can be due to defects in vestibular neurons and accessory structures (Anagnostopoulos, 2002). We found that in some $Chd7^{Gt/+}$ mice, vestibular hair cells were present despite absence of vestibular nerve innervation. Posterior cristae of some $Chd7^{Gt/+}$ mice contained hair cells even though nerve calyces were missing. The presence of sensory cells in the absence of afferent innervation has implications for the mechanisms of hair cell differentiation and survival. Prior studies in various experimental model systems have demonstrated that hair cells can develop and differentiate normally in the absence of neurons. Normal vestibular hair cell differentiation occurs in denervated embryonic chicken ears (Corwin and Cotanche, 1989), and fully formed, mature cochlear outer hair cells are present in mouse strains with severe nerve fiber loss, such as the neurotrophin-3 (NT-3) null mutant (Fritzsch et al., 2004).

Together, these findings suggest that hair cell development is not dependent on neuron-directed influence. Here we show that vestibular hair cells can survive into relatively advanced ages (11 months) without associated innervation. The persistence of mature hair cells in the absence of afferent innervation suggests that innervation is not necessary for long-term vestibular hair cell survival. This may be of importance for clinical interventions aimed at inducing nerve growth toward the denervated hair cells. It is not known whether reduced or absent innervation of the posterior crista in $Chd7^{Gt/+}$ mice is due to absence of primary vestibular neurons or lack of appropriate signaling from the sensory epithelium.

Comparisons with other *Chd7*-deficient mice

Some of the gross morphologic and behavioral abnormalities of $Chd7^{Gt/+}$ mice are similar to those found in other heterozygous *Chd7*-deficient lines derived from ENU mutagenesis (Bosman et al., 2005). Similarities include variability in semicircular canal defects between mice and between right and left ears of the same mouse, as well as defects of the non-ampullated end of the lateral canals (Bosman et al., 2005; Hurd et al., 2007). In $Chd7^{Gt/+}$ mice, the lateral crista was usually present, although in a few ears, the lateral ampulla was missing whereas a portion of the anterior end of the lateral canal remained. Other *Chd7*-deficient mice also have variable posterior canal defects, ranging from the canal and ampullae being reduced in size to being completely absent (Bosman et al., 2005; Hurd et al., 2007). Defects in the posterior crista and its innervation in $Chd7^{Gt/+}$ mice occur despite an intact posterior canal and intact hair cells. This is of interest both for understanding developmental mechanisms and for designing therapies.

Mutations leading to semicircular canal abnormalities have been identified in at least 24 mouse genes (Anagnostopoulos, 2002). Some of these genes (*BMP4*, *Jagged1*, *Fgf10*, *EphB2*) encode signaling molecules that may be direct targets of CHD7 transcriptional regulation (Cowan et al., 2000; Tsai et al., 2001; Pauley et al., 2003; Thompson et al., 2003). Genes that encode proteins whose primary function is in the cell nucleus (*Otx1*, *Hmx3/Nkx5.1*, *Prx1/2*, *Hoxa2*, *Hoxa1/b1*, *Nor-1*, *Dlx5*, *Gbx2*, *Pou3f4*, *Foxg1*, *Fkh10*, *kr/mafB*, *Sox2*) may also be targets of CHD7 transcription, or may act as protein-protein interacting partners in CHD7 complexes (Gavalas et al., 1998; Hulander et al., 1998; Morsli et al., 1998; ten Berge et al., 1998; Wang et al., 1998, 2004; Acampora et al., 1999; Depew et al., 1999; Phippard et al., 1999; Rossel and Capecchi, 1999; Ponnio et al., 2002; Kiernan et al., 2005; Lin et al., 2005; Pauley et al., 2006; Choo et al., 2006). Aside from *Chd7*, only a few other genes (*Hmx2/3*, *Dlx5*, *Fgf10*) are known to be critical for development of both the semicircular canals and their cristae (Wang et al., 1998, 2004; Pauley et al., 2003; Chang et al., 2004).

The time course of vestibular organ development and gene expression likely influences the nature and severity of inner ear defects in both humans and mice. In mice, the semicircular canals are formed between embryonic days 11.5 and 13 (Martin and Swanson, 1993). The anterior and posterior semicircular canals develop from a common vertical outpouching in the dorsal otocyst, whereas the lateral canal develops from a horizontal outpouching in the middle part of the otocyst (Morsli et al., 1998). $Chd7^{Gt/+}$ mice have consistent defects of the lateral semicircular canal, ranging from truncations to reduced loop or birdbeak-shaped canals. The lateral semicircular canal is the last canal to form in mice and humans and is the most common canal disrupted in humans (Jackler et al., 1987). The lateral canal is also the most commonly disrupted canal in *Chd7*-deficient mice, raising the possibility that *Chd7* is required for cellular proliferation, survival, or differentiation during the critical period of lateral canal development. *CHD7* may also have a similar role in human semicircular canal development. In mice, the posterior crista forms at embryonic day 11.5, followed by the anterior and lateral cristae and the macula utriculi at embryonic day 12 (Morsli et al., 1998). The anterior and lateral cristae are believed to share a common developmental origin (Morsli et al., 1998). In $Chd7^{Gt/+}$ mice with a missing lateral ampulla, the associated crista ampullaris is typically also missing.

The complex nature of the developing inner ear may involve direct signaling between sensory epithelia and their associated semicircular canals. Fibroblast growth factors expressed by the sensory cristae influence the outgrowth of semicircular canals, and it is thought that canal development requires prior specification by sensory tissues (Chang et al., 2004). However, there is also evidence that canal development is required for proper formation of the sensory epithelia. *Foxg1* null mice develop lateral semicircular canals despite the absence of a lateral crista (Pauley et al., 2006). Because the anterior and lateral crista share a common developmental origin, the anterior crista may be required for the formation of both the lateral and anterior semicircular canals.

$Chd7^{Gt/+}$ mutant mice have intact lateral cristae but severely malformed lateral semicircular canals. Given these observations, it is difficult to explain why the posterior cristae of $Chd7^{Gt/+}$ mice have abnormal structure and innervation without more severe disruptions of the

posterior canal. To our knowledge, *Chd7*$^{Gt/+}$ mice are the first mutant mice in which formation of the posterior crista is abnormal despite an intact posterior semicircular canal. This observation suggests that a complicated signaling relationship between the sensory and non-sensory epithelium is critical for correct inner ear morphogenesis. Because many earlier studies used in situ hybridization or other histological approaches to analyze inner ear epithelia of mutant mice, it is also possible that subtler defects in the subcellular organization of the sensory epithelium organization might have been missed.

Inter- and intra-animal variability

We observed considerable variability in canal morphology, sensory epithelial morphology, and posterior crista innervation between *Chd7*$^{Gt/+}$ mice and between right and left ears of the same mice. This variable expressivity is characteristic of CHARGE syndrome in humans (Aramaki et al., 2006). The reasons for asymmetry of mammalian *Chd7* inner ear phenotypes are not clear. We hypothesize that the array of lateral canal defects and posterior crista morphologies represents a continuum of phenotypic expression of *Chd7* mutations, with the loop canal and rudimentary sensory epithelia being the mildest forms and the truncation and patch-like epithelium being the most severe. *Chd7* likely has pleiotropic effects during development, and it is possible that the ear has a unique dosage requirement for *Chd7*. The observed right-left variability within a given *Chd7*$^{Gt/+}$ mouse is also consistent with prevailing epigenetic influences or altered expression of right/left body symmetry genes. Further studies using conditional *Chd7* alleles will help distinguish among these possibilities.

Circling behaviors

In *Chd7*$^{Gt/+}$ mice, truncation or narrowing of the lateral canal is correlated with circling behavior, whereas the presence of a complete canal is not. The lack of circling behavior in one mouse with bilateral lateral canal truncations and others with unilateral bird-beaks is notable. This mouse may have had subtler head bobbing behaviors not detected in our analysis or might harbor a suppressor mutation in a *Chd7* modifier gene(s). Also, although one mouse with bilaterally absent posterior canals circled, asymmetric posterior canal defects and bilateral complete posterior canals were noted in circling and non-circling mice. Similarly, some mice lacking innervation of the posterior cristae circled, whereas others did not. Thus, the data are insufficient to attribute the circling to any one single cause or site of pathology in the sensory epithelium.

Many strains of circling mice have inner ear defects, but some circling mutant mice lack structural abnormalities of the inner ear, suggesting that central or other peripheral lesions may cause or contribute to circling behavior (Nolan et al., 1995; Rabbath et al., 2001). Several parameters of the circling behavior may shed light on its origins. These include the uni- versus bi-directionality of the circling, the extent to which circling continues throughout life, correlations with the presence of hair cells, and the relationship to other positional pathologies such as head bobbing or shaking. Many circling mice have severe hearing loss, but at least one *Chd7*-deficient strain (*Edy*/+) has only mildly raised compound action potentials, which indicates normal function of hair cells (Kiernan et al., 2002). Therefore, it is possible that *Chd7*-deficient vestibular hair cells are functional and could be stimulated to provide signals to the central nervous system. The presence of circling in other mutant mice with profound bilateral inner ear dysfunction (*pirouette*, *spinner*) also suggests that unilateral or asymmetric inner ear defects are not required for circling (Beyer et al., 2000; Mitchem et al., 2002). Further studies will determine the contribution of vestibular nerve function as well as visual, cerebellar, and basal ganglia involvement in the circling behaviors of *Chd7*$^{Gt/+}$ deficient mice. Correlations between circling mice and an inner ear phenotype have been examined in other mouse mutants. All circling *Ecl* mice display bilateral lateral semicircular canal malformations, which vary in severity among animals and between ears of the same animal (Cryns et al., 2004). This is consistent with what we have observed with *Chd7*$^{Gt/+}$ mice.

Cellular functions of *Chd7* in vestibular phenotypes

Chd7 is a member of the chromodomain family of proteins that are proposed to regulate chromatin via ATP-dependent helicase and DNA binding activities (Woodage et al., 1997). *Chd7* also has important protein-protein interaction domains (SANT and BRK), which likely contribute to its functional roles (Woodage et al., 1997). The interacting proteins and downstream target genes of *Chd7* are not known, but clues can be obtained from other organisms. In *Drosophila melanogaster*, the *Chd7* orthologue *kismet* functions as a transcriptional activator, with important roles in transcriptional elongation by RNA polymerase II and in maintaining segmental identity during development (Daubresse et al., 1999). We hypothesize that *Chd7* activates transcription of genes that are critical for inner ear development. Additional studies are needed to identify these downstream target genes, some of which may also be required for normal inner ear development.

Genetic background effects

Chd7$^{Gt/+}$ mice were derived from a mixed 129 genetic background and have been backcrossed two generations onto either C57BL/6J or 129S1/SvImJ. Most *Chd7*$^{Gt/+}$ mice examined in this study were backcrossed to C57BL/6J mice, which are known to develop age-related hearing loss (*ahl*) due to mutations in *cadherin-23* (Noben-Trauth et al., 2003). This modifying *cadherin-23* gene mutation leads to reduced hearing in some C57BL/6J mice older than 1 year of age, is thought to be related to cochlear hair cell loss, and is not associated with circling (Noben-Trauth et al., 2003). Although the number of *Chd7*$^{Gt/+}$ mice on the 129S1/SvImJ background that were analyzed in this study is small, similar inner ear defects were seen in the 129S1/SvImJ and C57BL/6J genetic backgrounds. This may be due to the high genetic similarities between these mice, which are only two generations away from the original founders. Further backcrossing to these different strains may uncover genetic background effects such as those seen in *Wheels*, a mouse mutant that maps to chromosome 4 but has not been proved to have a *Chd7* mutation (Bosman et al., 2005). *Wheels* mice exhibit 99% circling behaviors on a C57BL6/J background and 25% circling on a hybrid background (Nolan et al., 1995).

Clinical relevance

Inner ear defects manifest more consistently than other clinical features in CHARGE individuals and are therefore useful for diagnosis (Amiel et al., 2001). The vestibular problems appear to be a dominant co-morbidity in CHARGE patients, who experience postural and motor difficulties throughout their lives (Abadie et al., 2000). Thus the use of *Chd7* mutant mouse models is important for understanding this vestibular pathology. We describe several findings that are common to $Chd7^{Gt/+}$ mice and CHARGE patients. Similar to humans, all mice with *Chd7* mutations have vestibular defects. Specific findings common to CHARGE patients and $Chd7^{Gt/+}$ mice are partial or complete semicircular canal hypoplasia, reduced canal function, asymmetric defects, and substantial variability between ears and between subjects, even among siblings (Tellier et al., 1998; Jongmans et al., 2006; Morimoto et al., 2006). Our mouse studies also suggest that vestibular sensory epithelia may be disrupted in CHARGE individuals.

Some of our findings raise possibilities for future therapies. The presence of hair cells without innervation in the posterior cristae suggests that therapies aimed at attracting growth of neurons toward hair cells in the sensory epithelium may be beneficial. The presence of an intact lateral crista in the ampulla of a defective lateral canal implies that novel surgical treatments to shunt endolymphatic fluid via an artificial canal could promote fluid movement though the ampulla. Such a "canal-plasty" might result in stimulation of the intact lateral sensory epithelium and restore function. Future studies will be aimed at exploring these therapeutic options and uncovering the mechanisms whereby *Chd7* regulates early developmental events in the semicircular canals and related vestibular tissues.

ACKNOWLEDGMENTS

We thank Mark Crumling for valuable discussion and Kate Barald and Dave Kohrman for their critical review of the manuscript.

LITERATURE CITED

Abadie V, Wiener-Vacher S, Morisseau-Durand MP, Poree C, Amiel J, Amanou L, Peigne C, Lyonnet S, Manac'h Y. 2000. Vestibular anomalies in CHARGE syndrome: investigations on and consequences for postural development. Eur J Pediatr 159:569–574.

Acampora D, Merlo GR, Paleari L, Zerega B, Postiglione MP, Mantero S, Bober E, Barbieri O, Simeone A, Levi G. 1999. Craniofacial, vestibular and bone defects in mice lacking the Distal-less-related gene *Dlx5*. Development 126:3795–3809.

Amiel J, Attiee-Bitach T, Marianowski R, Cormier-Daire V, Abadie V, Bonnet D, Gonzales M, Chemouny S, Brunelle F, Munnich A, Manach Y, Lyonnet S. 2001. Temporal bone anomaly proposed as a major criteria for diagnosis of CHARGE syndrome. Am J Med Genet 99:124–127.

Anagnostopoulos AV. 2002. A compendium of mouse knockouts with inner ear defects. Trends Genet 18:499.

Aramaki M, Udaka T, Kosaki R, Makita Y, Okamoto N, Yoshihashi H, Oki H, Nanao K, Moriyama N, Oku S, Hasegawa T, Takahashi T, Fukushima Y, Kawame H, Kosaki K. 2006. Phenotypic spectrum of CHARGE syndrome with *CHD7* mutations. J Pediatr 148:410–414.

Barald KF, Kelley MW. 2004. From placode to polarization: new tunes in inner ear development. Development 131:4119–4130.

Berglund AM, Ryugo DK. 1991. Neurofilament antibodies and spiral ganglion neurons of the mammalian cochlea. J Comp Neurol 306:393–408.

Beyer LA, Odeh H, Probst FJ, Lambert EH, Dolan DF, Camper SA, Kohrman DC, Raphael Y. 2000. Hair cells in the inner ear of the *pirouette* and *shaker 2* mutant mice. J Neurocytol 29:227–240.

Bosman EA, Penn AC, Ambrose JC, Kettleborough R, Stemple DL, Steel KP. 2005. Multiple mutations in mouse Chd7 provide models for CHARGE syndrome. Hum Mol Genet 14:3463–3476.

Byerly KA, Pauli RM. 1993. Cranial nerve abnormalities in CHARGE association [see comments]. Am J Med Genet 45:751–757.

Chang W, Brigande JV, Fekete DM, Wu DK. 2004. The development of semicircular canals in the inner ear: role of FGFs in sensory cristae. Development 131:4201–4211.

Choo D, Ward J, Reece A, Dou H, Lin Z, Greinwald J. 2006. Molecular mechanisms underlying inner ear patterning defects in *kreisler* mutants. Dev Biol 289:308–317.

Corwin JT, Cotanche DA. 1989. Development of location-specific hair cell stereocilia in denervated embryonic ears. J Comp Neurol 288:529–537.

Cowan CA, Yokoyama N, Bianchi LM, Henkemeyer M, Fritzsch B. 2000. EphB2 guides axons at the midline and is necessary for normal vestibular function. Neuron 26:417–430.

Cryns K, van Alphen AM, van Spaendonck MP, van de Heyning PH, Timmermans JP, de Zeeuw CI, van Camp G. 2004. Circling behavior in the *Ecl* mouse is caused by lateral semicircular canal defects. J Comp Neurol 468:587–595.

Dau J, Wenthold RJ. 1989. Immunocytochemical localization of neurofilament subunits in the spiral ganglion of normal and neomycin-treated guinea pigs. Hear Res 42:253–263.

Daubresse G, Deuring R, Moore L, Papoulas O, Zakrajsek I, Waldrip WR, Scott MP, Kennison JA, Tamkun JW. 1999. The *Drosophila kismet* gene is related to chromatin-remodeling factors and is required for both segmentation and segment identity. Development 126:1175–1187.

Depew MJ, Liu JK, Long JE, Presley R, Meneses JJ, Pedersen RA, Rubenstein JL. 1999. *Dlx5* regulates regional development of the branchial arches and sensory capsules. Development 126:3831–3846.

Desai SS, Ali H, Lysakowski A. 2005a. Comparative morphology of rodent vestibular periphery. II. Cristae ampullares. J Neurophysiol 93:267–280.

Desai SS, Zeh C, Lysakowski A. 2005b. Comparative morphology of rodent vestibular periphery. I. Saccular and utricular maculae. J Neurophysiol 93:251–266.

Fekete DM. 1996. Cell fate specification in the inner ear. Curr Opin Neurobiol 6:533–541.

Fritzsch B, Tessarollo L, Coppola E, Reichardt LF. 2004. Neurotrophins in the ear: their roles in sensory neuron survival and fiber guidance. Prog Brain Res 146:265–278.

Fritzsch B, Pauley S, Matei V, Katz DM, Xiang M, Tessarollo L. 2005. Mutant mice reveal the molecular and cellular basis for specific sensory connections to inner ear epithelia and primary nuclei of the brain. Hear Res 206:52–63.

Gavalas A, Studer M, Lumsden A, Rijli FM, Krumlauf R, Chambon P. 1998. *Hoxa1* and *Hoxb1* synergize in patterning the hindbrain, cranial nerves and second pharyngeal arch. Development 125:1123–1136.

Goldberg JM, Baird RA, Fernandez C. 1985. Morphophysiological studies of the mammalian vestibular labyrinth. Prog Clin Biol Res 176:231–245.

Goldberg JM, Lysakowski A, Fernandez C. 1990. Morphophysiological and ultrastructural studies in the mammalian cristae ampullares. Hear Res 49:89–102.

Hulander M, Wurst W, Carlsson P, Enerback S. 1998. The winged helix transcription factor Fkh10 is required for normal development of the inner ear. Nat Genet 20:374–376.

Hurd EA, Capers PL, Blauwkamp MN, Adams ME, Raphael Y, Poucher HK, Martin DM. 2007. Loss of Chd7 function in gene-trapped reporter mice is embryonic lethal and associated with severe defects in multiple developing tissues. Mamm Genome 18:94–104.

Issekutz KA, Graham JM Jr, Prasad C, Smith IM, Blake KD. 2005. An epidemiological analysis of CHARGE syndrome: preliminary results from a Canadian study. Am J Med Genet A 133:309–317.

Jackler RK, Luxford WM, House WF. 1987. Congenital malformations of the inner ear: a classification based on embryogenesis. Laryngoscope 97(Suppl 40):2–14.

Johnson DS, Morrison N, Grant L, Turner T, Fantes J, Connor JM, Murday VA. 2006. Confirmation of *CHD7* as a cause of CHARGE association identified by mapping a balanced chromosome translocation in affected monozygotic twins. J Med Genet 43(3):280–284.

Jongmans MC, Admiraal RJ, van der Donk KP, Vissers LE, Baas AF,

Kapusta L, van Hagen JM, Donnai D, de Ravel TJ, Veltman JA, Geurts van Kessel A, De Vries BB, Brunner HG, Hoefsloot LH, van Ravenswaaij CM. 2006. CHARGE syndrome: the phenotypic spectrum of mutations in the *CHD7* gene. J Med Genet 43:306–314.

Kallen K, Robert E, Mastroiacovo P, Castilla EE, Kallen B. 1999. CHARGE association in newborns: a registry-based study. Teratology 60:334–343.

Kiernan AE, Erven A, Voegeling S, Peters J, Nolan P, Hunter J, Bacon Y, Steel KP, Brown SD, Guenet JL. 2002. ENU mutagenesis reveals a highly mutable locus on mouse chromosome 4 that affects ear morphogenesis. Mamm Genome 13:142–148.

Kiernan AE, Pelling AL, Leung KK, Tang AS, Bell DM, Tease C, Lovell-Badge R, Steel KP, Cheah KS. 2005. *Sox2* is required for sensory organ development in the mammalian inner ear. Nature 434:1031–1035.

Lalani SR, Safiullah AM, Fernbach SD, Harutyunyan KG, Thaller C, Peterson LE, McPherson JD, Gibbs RA, White LD, Hefner M, Davenport SL, Graham JM, Bacino CA, Glass NL, Towbin JA, Craigen WJ, Neish SR, Lin AE, Belmont JW. 2006. Spectrum of *CHD7* mutations in 110 individuals with CHARGE syndrome and genotype-phenotype correlation. Am J Hum Genet 78:303–314.

Lin AE, Siebert JR, Graham JM Jr. 1990. Central nervous system malformations in the CHARGE association. Am J Med Genet 37:304–310.

Lin Z, Cantos R, Patente M, Wu DK. 2005. *Gbx2* is required for the morphogenesis of the mouse inner ear: a downstream candidate of hindbrain signaling. Development 132:2309–2318.

Martin P, Swanson GJ. 1993. Descriptive and experimental analysis of the epithelial remodellings that control semicircular canal formation in the developing mouse inner ear. Dev Biol 159:549–558.

Meiteles LZ, Raphael Y. 1994. Distribution of cytokeratins in the vestibular epithelium of the guinea pig. Ann Otol Rhinol Laryngol 103:149–155.

Mitchem KL, Hibbard E, Beyer LA, Bosom K, Dootz GA, Dolan DF, Johnson KR, Raphael Y, Kohrman DC. 2002. Mutation of the novel gene *Tmie* results in sensory cell defects in the inner ear of spinner, a mouse model of human hearing loss DFNB6. Hum Mol Genet 11:1887–1898.

Morimoto AK, Wiggins RH 3rd, Hudgins PA, Hedlund GL, Hamilton B, Mukherji SK, Telian SA, Harnsberger HR. 2006. Absent semicircular canals in CHARGE syndrome: radiologic spectrum of findings. AJNR Am J Neuroradiol 27:1663–1671.

Morsli H, Choo D, Ryan A, Johnson R, Wu DK. 1998. Development of the mouse inner ear and origin of its sensory organs. J Neurosci 18:3327–3335.

Noben-Trauth K, Zheng QY, Johnson KR. 2003. Association of cadherin 23 with polygenic inheritance and genetic modification of sensorineural hearing loss. Nat Genet 35:21–23.

Nolan PM, Sollars PJ, Bohne BA, Ewens WJ, Pickard GE, Bucan M. 1995. Heterozygosity mapping of partially congenic lines: mapping of a semidominant neurological mutation, *Wheels* (*Whl*), on mouse chromosome 4. Genetics 140:245–254.

Osborne MP, Comis SD. 1991. Preparation of inner ear sensory hair bundles for high resolution scanning electron microscopy. Scanning Microsc 5:555–564.

Osborne MP, Comis SD, Pickles JO. 1984. Morphology and cross-linkage of stereocilia in the guinea-pig labyrinth examined without the use of osmium as a fixative. Cell Tissue Res 237:43–48.

Pauley S, Wright TJ, Pirvola U, Ornitz D, Beisel K, Fritzsch B. 2003. Expression and function of FGF10 in mammalian inner ear development. Dev Dyn 227:203–215.

Pauley S, Lai E, Fritzsch B. 2006. *Foxg1* is required for morphogenesis and histogenesis of the mammalian inner ear. Dev Dyn 235:2470–2482.

Phippard D, Lu L, Lee D, Saunders JC, Crenshaw EB 3rd. 1999. Targeted mutagenesis of the POU-domain gene *Brn4*/*Pou3f4* causes developmental defects in the inner ear. J Neurosci 19:5980–5989.

Ponnio T, Burton Q, Pereira FA, Wu DK, Conneely OM. 2002. The nuclear receptor Nor-1 is essential for proliferation of the semicircular canals of the mouse inner ear. Mol Cell Biol 22:935–945.

Rabbath G, Necchi D, de Waele C, Gasc JP, Josset P, Vidal PP. 2001. Abnormal vestibular control of gaze and posture in a strain of a waltzing rat. Exp Brain Res 136:211–223.

Raphael Y, Athey BD, Wang Y, Lee MK, Altschuler RA. 1994. F-actin, tubulin and spectrin in the organ of Corti: comparative distribution in different cell types and mammalian species. Hear Res 76:173–187.

Rossel M, Capecchi MR. 1999. Mice mutant for both *Hoxa1* and *Hoxb1* show extensive remodeling of the hindbrain and defects in craniofacial development. Development 126:5027–5040.

Sanlaville D, Etchevers HC, Gonzales M, Martinovic J, Clement-Ziza M, Delezoide AL, Aubry MC, Pelet A, Chemouny S, Cruau C, Audollent S, Esculpavit C, Goudefroye G, Ozilou C, Fredouille C, Joye N, Morichon-Delvallez N, Dumez Y, Weissenbach J, Munnich A, Amiel J, Encha-Razavi F, Lyonnet S, Vekemans M, Attie-Bitach T. 2006. Phenotypic spectrum of CHARGE syndrome in fetuses with *CHD7* truncating mutations correlates with expression during human development. J Med Genet 43(3):211–217.

Tellier AL, Cormier-Daire V, Abadie V, Amiel J, Sigaudy S, Bonnet D, de Lonlay-Debeney P, Morrisseau-Durand MP, Hubert P, Michel JL, Jan D, Dollfus H, Baumann C, Labrune P, Lacombe D, Philip N, LeMerrer M, Briard ML, Munnich A, Lyonnet S. 1998. CHARGE syndrome: report of 47 cases and review. Am J Med Genet 76:402–409.

ten Berge D, Brouwer A, Korving J, Martin JF, Meijlink F. 1998. *Prx1* and *Prx2* in skeletogenesis: roles in the craniofacial region, inner ear and limbs. Development 125:3831–3842.

Thompson DL, Gerlach-Bank LM, Barald KF, Koenig RJ. 2003. Retinoic acid repression of bone morphogenetic protein 4 in inner ear development. Mol Cell Biol 23:2277–2286.

Tsai H, Hardisty RE, Rhodes C, Kiernan AE, Roby P, Tymowska-Lalanne Z, Mburu P, Rastan S, Hunter AJ, Brown SD, Steel KP. 2001. The mouse slalom mutant demonstrates a role for *Jagged1* in neuroepithelial patterning in the organ of Corti. Hum Mol Genet 10:507–512.

Verloes A. 2005. Updated diagnostic criteria for CHARGE syndrome: a proposal. Am J Med Genet A 133:306–308.

Vissers LE, van Ravenswaaij CM, Admiraal R, Hurst JA, de Vries BB, Janssen IM, van der Vliet WA, Huys EH, de Jong PJ, Hamel BC, Schoenmakers EF, Brunner HG, Veltman JA, van Kessel AG. 2004. Mutations in a new member of the chromodomain gene family cause CHARGE syndrome. Nat Genet 36:955–957.

Wang W, Van De Water T, Lufkin T. 1998. Inner ear and maternal reproductive defects in mice lacking the *Hmx3* homeobox gene. Development 125:621–634.

Wang W, Grimmer JF, Van De Water TR, Lufkin T. 2004. *Hmx2* and *Hmx3* homeobox genes direct development of the murine inner ear and hypothalamus and can be functionally replaced by *Drosophila Hmx*. Dev Cell 7:439–453.

Woodage T, Basrai MA, Baxevanis AD, Hieter P, Collins FS. 1997. Characterization of the CHD family of proteins. Proc Natl Acad Sci U S A 94:11472–11477.